ELSEVIER

Earth and Planetary Science Letters 193 (2001) 1–12

EPSL

www.elsevier.com/locate/epsl

Contradictory magnetic polarities in sediments and variable timing of neoformation of authigenic greigite

Wei-Teh Jiang [a,*], Chorng-Shern Horng [b], Andrew P. Roberts [c], Donald R. Peacor [d]

[a] *Department of Earth Sciences, National Cheng Kung University, Tainan 70101, Taiwan*
[b] *Institute of Earth Sciences, Academia Sinica, P.O. Box 1-55, Nankang, Taipei, Taiwan*
[c] *School of Ocean and Earth Science, University of Southampton, Southampton Oceanography Centre, European Way, Southampton SO14 3ZH, UK*
[d] *Department of Geological Sciences, University of Michigan, Ann Arbor, MI 48109-1063, USA*

Received 29 May 2001; received in revised form 25 August 2001; accepted 5 September 2001

Abstract

In several recent published studies, paleomagnetic results from greigite-bearing sediments reveal characteristic remanences that are anti-parallel to those carried by coexisting detrital magnetic minerals and polarities that are opposite to those expected for the age of the rock unit. These observations have important implications for the reliability of paleomagnetic data from greigite-bearing sediments. We have investigated the origin of such contradictory magnetic polarities by studying the formation mechanisms of greigite in mudstones from the Lower Gutingkeng Formation, southwestern Taiwan. Scanning electron microscope observations indicate that the Gutingkeng greigite has three modes of occurrence, including nodular, framboidal and matrix greigite. Microtextural observations, including transection of bedding by iron-sulfide nodules with no deviation of sediment textures, the presence of partially dissolved edges around detrital and early diagenetic phases, and neoformation of greigite and Fe-rich clays around detrital phyllosilicates, indicate that all three types of greigite have a diagenetic origin that post-dates early diagenetic pyrite. In addition, paleomagnetic data yield contradictory polarities even for greigite-bearing sister samples from the same stratigraphic horizon. The data are collectively interpreted to indicate that neoformation of the Gutingkeng greigite occurred after partial dissolution of syngenetic or early diagenetic pyrite. The timing of greigite formation can apparently vary enough to give contradictory polarities for different greigite components even within a single stratigraphic horizon. Direct petrographic observation of authigenic magnetic iron-sulfide phases, as carried out in this study, can provide important constraints on formation mechanisms and timing of remanence acquisition for these minerals and suggests that care should be taken when interpreting magnetostratigraphic data from greigite-bearing sediments.

Keywords: greigite; pyrite; magnetite; mudstone; framboidal texture; nodules; magnetization; Taiwan

* Corresponding author. Tel.: +886-6-2757575 ext. 65437; Fax: +886-6-2740285.
E-mail addresses: atwtj@sparc3.cc.ncku.edu.tw (W.-T. Jiang), cshorng@earth.sinica.edu.tw (C.-S. Horng), arob@mail.soc.soton.ac.uk (A.P. Roberts), drpeacor@umich.edu (D.R. Peacor).

0012-821X/01/$ – see front matter
PII: S0012-821X(01)00497-6

1. Introduction

Greigite (Fe_3S_4) is a minor but potentially important magnetic constituent of many marine sediments. Along with other sulfides, such as pyrite and pyrrhotite, it plays a major role in the geochemical cycling of O, C, N and S. Greigite formation is usually related to early diagenetic, reducing conditions [1–7], although it can form during later diagenesis depending on the diagenetic environment [5]. Greigite is ferrimagnetic and its natural remanent magnetization (NRM) is potentially important for paleomagnetic studies. In several reported instances, paleomagnetic results from greigite-bearing sediments have yielded polarities opposite either to that expected for the age of the rock unit or opposite to that indicated by coexisting detrital magnetic minerals [7–9]. More than one generation of greigite has been reported within some sedimentary rocks, including early diagenetic and epigenetic greigite, which will have important implications for the NRM recorded by such rocks [3–5]. The interpretations of the above studies have generally been based on paleomagnetic measurements, with independent identification of greigite, and occasionally with assistance from sulfur isotopic data. In this study, we address the problem of NRM acquisition arising from variable timing of greigite formation by describing detailed electron microscopic observations from sediments for which the polarities of detrital magnetite and authigenic greigite have been demonstrated to be contradictory [9].

2. Geological setting and methods

The studied samples were collected from the lower portion of the Lower Gutingkeng Formation in the eastern segment of the Erhjen-chi (EJE) river section in southwestern Taiwan (Fig. 1). The Lower Gutingkeng Formation is a Plio–Pleistocene marine mudstone sequence and is about 1500 m thick in the EJE section [10]. Previous rock magnetic studies of three clastic sequences in the region have shown that detrital magnetite and authigenic greigite are widely distributed [9,11,12]. Thermal demagnetization results (25–400°C) from one sequence indicate that the polarities of greigite below 320–340°C are opposite to those revealed by detrital magnetite above 340°C [9]. The greigite is generally very fine-grained (<1 μm) and is dispersed throughout the matrix of the mudstones. It also occurs as aggregates of grains forming concretionary nodules of <1 to 5 mm in diameter (Fig. 2). Such nodules are sporadically distributed through the studied mudstone sequences and an early Pliocene portion of the nodule-bearing and surrounding sediments was investigated in more detail in the present study (Fig. 3).

X-ray diffraction (XRD) analysis (CuKα radiation operated at 40 kV and 30 mA) was performed to identify minerals from magnetic extracts and from powdered greigite nodules. Samples of about 100–200 g were crushed, stirred into a slurry, and pumped through the poles of an electromagnet with a peristaltic pump to obtain magnetic extracts (ca. 1–2‰ of the sample weight). Low-temperature (5–300 K) measurements of an isothermal remanent magnetization (IRM), imparted with a 1 T field at 5 K, were carried out in zero field on small bulk subsamples ($\sim$100 mg) as they were warmed to room temperature using a Quantum Design Magnetic Property Measurement System (MPMS-2). These measurements were conducted to enable detection of magnetic phase transitions for identification of magnetite or pyrrhotite [13–16]. The NRM was investigated to study the magnetic polarity of the sediments. Paleomagnetic measurements were made with a 2G Enterprises cryogenic magnetometer. Thermal demagnetization was conducted with an ASC thermal demagnetizer that has a low field (<10 nT) cooling chamber. The magnetometer and thermal demagnetizer are both located in a magnetically shielded room. Samples were heated from room temperature to 400°C in the following steps: 25, 120, 180, 240, 280, 300, 320, 340, 360, 380 and 400°C. Magnetic susceptibility was measured for selected samples after each heating step to monitor for thermal alteration.

A polished section of one of the nodule-bearing samples (EJEB380) was prepared for microtextural observations utilizing scanning electron micro-

scopes (SEMs) equipped with X-ray energy-dispersive spectrometers (EDSs) for elemental identification. The SEMs were operated at 15 or 20 kV, and back-scattered electron (BSE) images were digitally recorded with contrast relating to the densities and average atomic weights of mineral phases. Greigite normally has brighter contrast than pyrite in BSE images. This normal contrast was observed in the present study, but, in some cases, very fine-grained greigite shows slightly darker contrast than coarser-grained pyrite because of the relatively irregular scattering surface and possible intergrowth with or coating by silicates or other phases. Mineral identification was primarily based on EDS spectra in conjunction with XRD data.

3. Results

3.1. XRD and low-temperature IRM analyses

XRD analysis on magnetic extracts and on the powdered nodules indicates that greigite is the dominant magnetic carrier of the studied samples (Fig. 4). Pyrite coexists with greigite in variable ratios in the nodule-bearing samples, and quartz is common. Characteristic XRD peaks of pyrrhotite were not detected. In addition, a Verwey transition was detected at ca. 120 K in the low-temperature IRM measurements of all studied samples (Fig. 5). This suggests that magnetite is ubiquitous in these sediments, although it occurs only in low concentrations. The magnetic transition characteristic of pyrrhotite at ca. 30–35 K [13,14,16] was not detected in this study.

3.2. NRM

Representative thermal demagnetization data are shown in Fig. 6. They display either simple one-component or multiple-component NRMs. For samples with a simple one-component NRM, including samples from sites EJEB374, 375, 377 and 379, the remanence directions maintained normal polarity during the entire demag-

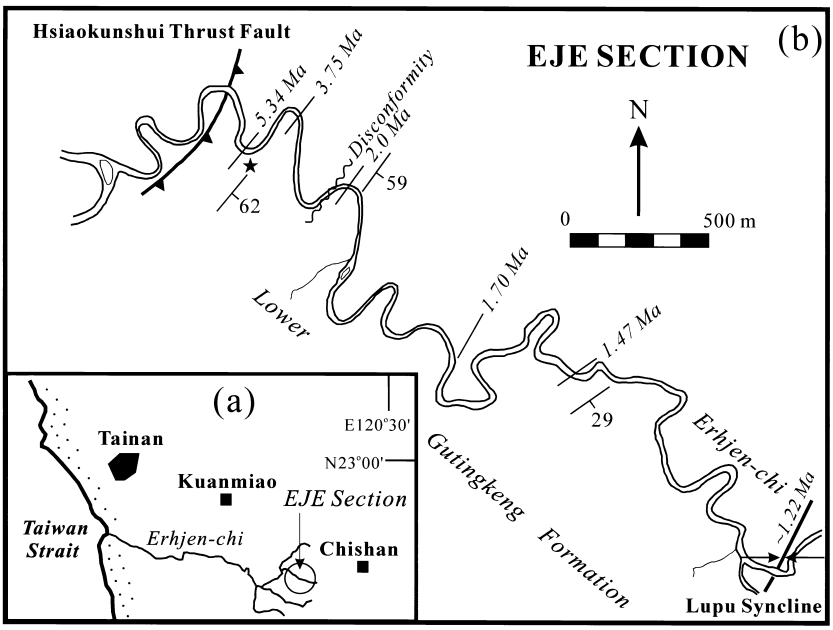

Fig. 1. (a) Location map of the eastern part of the EJE river section in southwestern Taiwan. (b) Map of the EJE section, showing bedding attitudes of the Lower Gutingkeng Formation and nannofossil datum ages based on Horng and Shea [10]. The star symbol indicates the locality of the studied early Pliocene greigite nodule-bearing sediments.

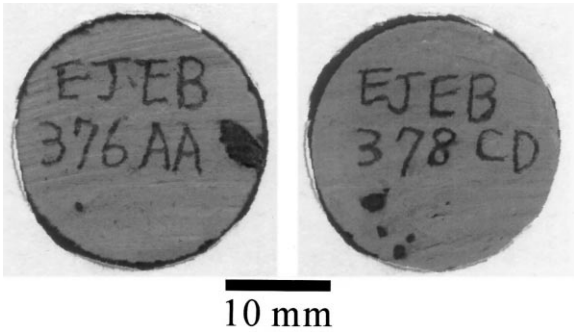

Fig. 2. Black iron-sulfide nodules, ranging from submillimeter to 5 mm in size, embedded in the gray mudstone matrix (samples from sites EJEB376 and EJEB378).

netization sequence (Fig. 6a). Samples from site 381 have a greater secondary remanence component but, nevertheless, normal polarity is also evident throughout the demagnetization sequence for this site (Fig. 6f). On the other hand, samples from sites EJEB376, 378 and 380 (except for EJEB380.GA) have more than one component of magnetization. For samples EJEB378.CB and EJEB380.GB, a reversed polarity component is isolated throughout a significant proportion of the unblocking temperature spectrum; an essentially anti-parallel normal polarity component is evident for the last one or two steps (Fig. 6c,e). Even for the two sister samples EJEB380.GA and EJEB380.GB, which were collected from the same core at the same stratigraphic level, the NRMs exhibit opposite polarities between 25 and 380°C

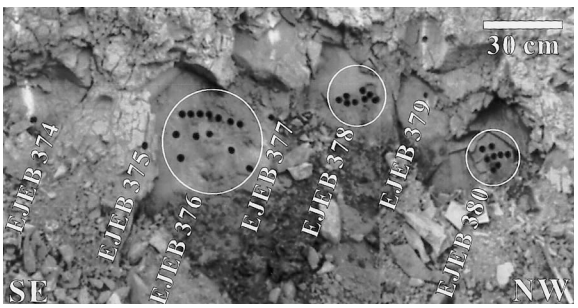

Fig. 3. Photograph of paleomagnetic sites from the EJE river section, where greigite-bearing nodules were found. Sampling sites are spaced at stratigraphic intervals of 30 cm or less. Detailed sampling was carried out at sites EJEB376, 378 and 380. The bedding plane is N40°E/62°SE, with southeast oriented to the left of the photograph.

(Fig. 6d,e). In summary, the NRM behavior of the samples in the temperature range of 25 to 380°C can be quite different between neighboring sites, or even in a single site. Regardless of the polarity below 380°C, any magnetization that persists to 380–400°C in these samples has normal polarity. Greigite does not persist to such high temperatures and readily transforms into pyrrhotite and pyrite [9,16–19]. The newly formed pyrrhotite may acquire a thermal remanent magnetization (TRM) and may affect the NRM direction, but the TRM acquisition is insignificant if the ambient field is well shielded during thermal demagnetization [9]. Thus, we infer that the normal polarity component is mainly contributed by detrital magnetite that was deposited during one of the early Pliocene normal polarity subchrons of the Gilbert Chron.

3.3. Microtextural observations

SEM observations indicate that the greigite has

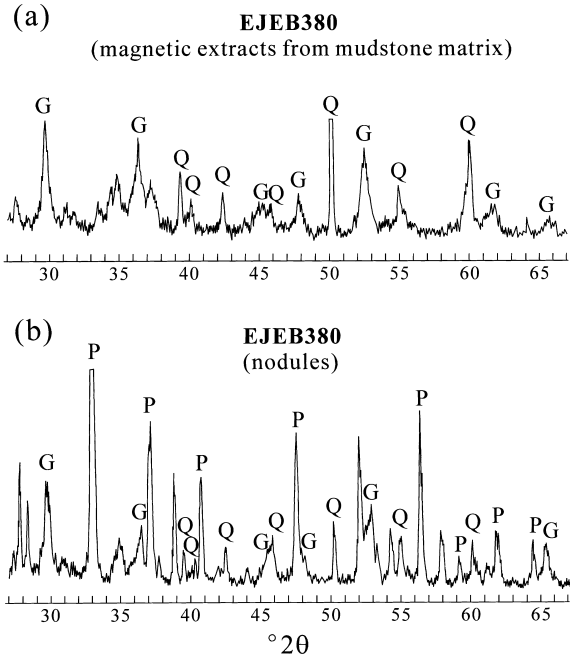

Fig. 4. XRD patterns of (a) magnetic extracts from mudstone matrix, and (b) powdered nodules, both from sample EJEB380. Characteristic peaks occur for greigite (G), pyrite (P) and quartz (Q).

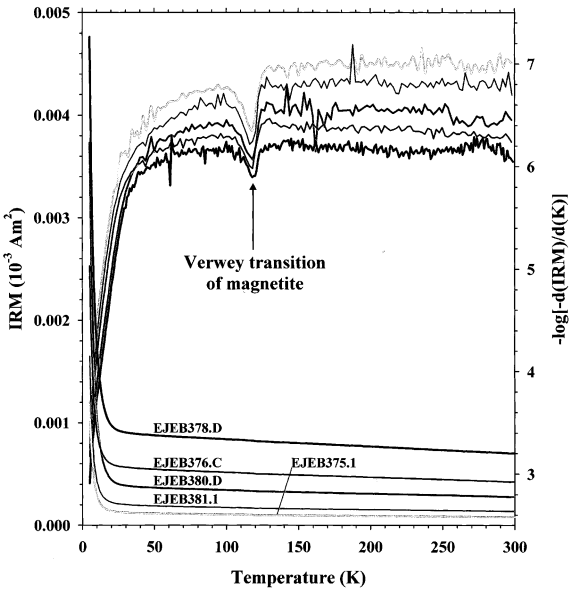

Fig. 5. Low-temperature analysis of IRM for small bulk samples, with measurements made during zero-field warming. The first derivative of the IRM with respect to temperature is expressed as $-\log[-d(IRM)/d(K)]$ with scales on the right-hand axis and data curves in the upper portion to illustrate the Verwey transition of magnetite at about 120 K.

three modes of occurrence, including: (1) fine-grained crystal aggregates in iron-sulfide nodules, (2) fine-grained crystal aggregates within pyrite aggregates surrounding pyrite framboids, and (3) small grains within phyllosilicate {001} cleavages or grains that are dispersed in the sediment matrix. These three textural types of greigite are hereafter referred to as nodular, framboidal and matrix greigite, respectively.

Nodular greigite occurs in iron-sulfide-dominated concretionary nodules surrounded by silicate-dominated matrix phases (Fig. 7a). The nodules have circular, elliptical, or irregularly elongated shapes in cross-section and contain abundant silicate grains with variable sizes. The silicate grains are embayed by pyrite, which is in turn enclosed by greigite aggregates having crystal sizes that are finer than the resolution limit of BSE images (Fig. 7b,c). Both embayed silicate and pyrite grains have partially dissolved edges. Intergrowths of greigite with fine-grained iron-rich clays frequently occur in the peripheral regions of nodules (Fig. 7d). The iron-rich clays (EDS spectra implying a mixture of Fe-rich chlorite and minor illite/smectite) occur only in the vicinity of greigite and they fill space between the greigite and silicate grains with corroded edges, consistent with an origin via diagenetic neoformation. The surrounding mudstone matrix exhibits no evidence of deformation or bending with respect to each nodule. EDS spectra of greigite have a high ratio of iron to sulfur compared to pyrite (Fig. 7e,f). Standardless calculations of the greigite and pyrite compositions suggest ca. 44% Fe (at%) and 56% S for greigite and ca. 34% Fe and 66% S for pyrite, consistent with the chemical formulae Fe_3S_4 and FeS_2, respectively. Nodular greigite is the most abundant of the three types of greigite in nodule-bearing samples.

Framboidal greigite occurs within irregularly elongated patches or aggregates of pyrite crystals that locally enclose spherical pyrite framboids (Fig. 8a). The pyrite aggregates consist of fine-grained crystals with submicron to ca. 1-μm diameter sizes. They fill space between silicate grains and have irregular boundaries in contact with the surrounding silicate-dominated matrix (Fig. 8b). Greigite crystals with sizes ranging from 0.1 to 0.5 μm form aggregates that occupy interstices between and around pyrite crystals within pyrite aggregates, and locally occur in the peripheral regions of pyrite framboids (Fig. 8c,d). Crystal edges of most of the framboidal pyrite crystals are not sharp, in contrast to those with well-defined crystal edges precipitated in other marine sediments (e.g. [20]).

Matrix greigite commonly occurs as separate submicron to ca. 1-μm grains dispersed in the matrix and locally forms arrays within detrital chlorite {001} cleavages (Fig. 9a). In some cases, fine-grained greigite forms aggregates that fill spaces between distorted packets of large detrital chlorite grains (Fig. 9b). Coarse-grained detrital muscovite is also present, but greigite occurs mostly in detrital chlorite grains. Magnetite was not observed by BSE imaging probably because its concentration is rather low, as suggested by the low-temperature IRM measurements and XRD data.

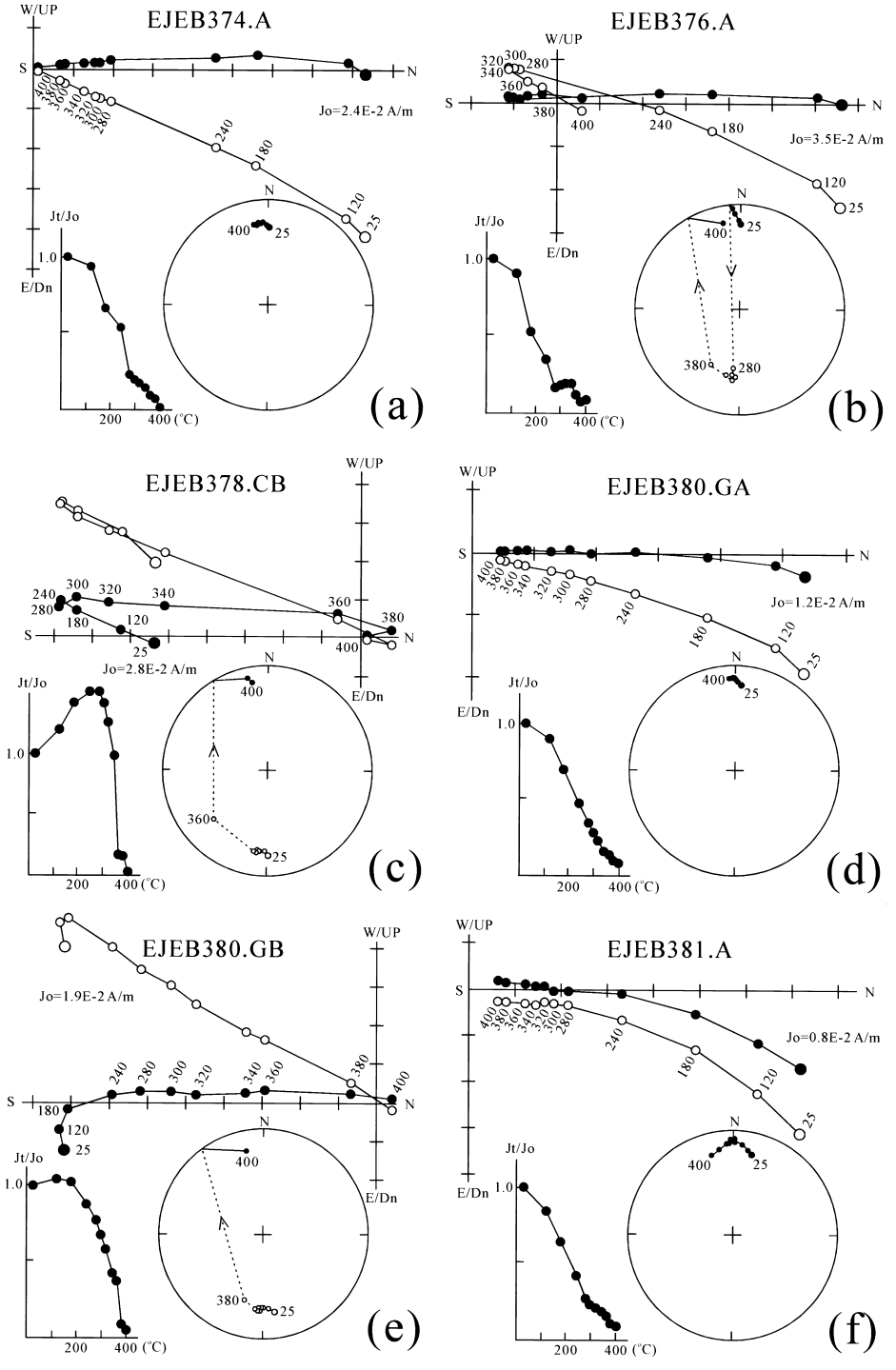
EJEB374.A
W/UP
S
N
Jo=2.4E-2 A/m
Jt/Jo
E/Dn
1.0
200
400 (°C)
(a)
EJEB376.A
W/UP
S
N
Jo=3.5E-2 A/m
Jt/Jo
E/Dn
1.0
200
400 (°C)
(b)
EJEB378.CB
W/UP
S
N
Jo=2.8E-2 A/m
Jt/Jo
E/Dn
1.0
200
400 (°C)
(c)
EJEB380.GA
W/UP
S
N
Jo=1.2E-2 A/m
Jt/Jo
E/Dn
1.0
200
400 (°C)
(d)
EJEB380.GB
W/UP
Jo=1.9E-2 A/m
S
N
Jt/Jo
E/Dn
1.0
200
400 (°C)
(e)
EJEB381.A
W/UP
S
N
Jo=0.8E-2 A/m
Jt/Jo
E/Dn
1.0
200
400 (°C)
(f)

Fig. 6. Representative vector-component diagrams for stepwise thermal demagnetization of samples from sites EJEB374 to EJEB381. The diagrams are plotted after application of a bedding correction (N40°E/62°SE). Solid circles, projection onto the horizontal plane; open circles, projection onto the vertical plane; J_0 = initial remanence intensity; J_t/J_0 = normalized remanence intensity. Thermal demagnetization paths are also shown on equal-area stereographic projections. Solid circles and lines, lower hemisphere projection; open circles and dashed lines, upper hemisphere projection.
←

4. Discussion

4.1. Diagenetic formation of greigite in iron-sulfide nodules

Three lines of evidence suggest that the iron-sulfide nodules in these sediments formed post-depositionally, including: (1) transection of bedding by nodules, with no deviation of sediment texture, (2) the presence of partially dissolved edges around numerous detrital silicate grains that are embayed by pyrite within or in the peripheral areas of the iron-sulfide nodules, (3) replacement of detrital phyllosilicates by greigite and neoformed Fe-rich clays in the vicinity of nodules. These features are consistent with diagenetic formation of sulfide nodules [21]. Pyrite grains within the nodules have partially dissolved edges and are enclosed by greigite aggregates, therefore the nodular greigite must also be diagenetic in origin, having formed subsequent to pyrite.

4.2. Post-depositional precipitation of greigite in pyrite framboids

Framboidal aggregates and euhedral crystals are common growth textures of pyrite in clastic sediments. The formation of framboidal pyrite is directly related to the production of hydrogen sulfide via bacterial reduction of sulfate in anoxic bottom waters and porewaters and to the availability of reactive iron-bearing minerals or aqueous species. Framboidal pyrite forms either diagenetically at shallow depths in normal marine sediments or syngenetically in anoxic bottom waters or at the sediment–water interface in euxinic environments, with or without the presence of precursor iron monosulfides. Pyrite tends to occur as small framboids or euhedral crystals at the surface of iron-bearing minerals during later stages of diagenesis when the availability of reactive iron-bearing species and/or sulfate in the porewaters is limited [1,2,20,22–28]. In the studied mudstones, spheroidal pyrite framboids could have formed syngenetically or diagenetically. The core–rim growth relationships imply that the surrounding finer grained pyrite aggregates or framboids of irregular shape formed after the spherical framboids. The occurrence of greigite framboids or aggregates in peripheral regions of spherical pyrite framboids and in interstices between pyrite crystals within pyrite aggregates suggests that the framboidal greigite formed after framboidal pyrite or contemporaneously with irregularly shaped pyrite aggregates.

4.3. Neoformation of matrix greigite

The common observation of neoformed greigite on or within layered phyllosilicate minerals implies that the layer surfaces of phyllosilicates are reactive sites for greigite formation. Such greigite occurrences may result from a build-up of sulfidic sulfur in pore waters at depth during diagenesis [25,26]. The reaction rates of iron-bearing phyllosilicate minerals toward dissolved sulfidic sulfur are much slower than for the highly reactive iron oxyhydroxides or iron oxides [25]. Early-formed sulfidic sulfur from bacterial sulfate reduction quickly reacts with iron oxyhydroxides or oxides to form iron sulfides and its reaction with iron-bearing phyllosilicate minerals occurs much later during diagenesis. The greigite associated with phyllosilicates in our sample (mostly chlorite) probably formed through later diagenetic reaction of iron in the phyllosilicates with sulfidic sulfur. The greigite that is sporadically dispersed in the matrix shows no evidence for the timing of formation, but its random spatial distribution might be consistent with formation at the same time as the greigite that is intervened with the phyllosilicate layers.

The microtextural data described above suggest that all three observed types of greigite formed diagenetically after pyrite formation. Post-depositional formation of greigite has been reported for a variety of marine sediments [3–6,8,9,19,29]. In the case of marine sediments from South Island, New Zealand, greigite was inferred to be a product of early diagenesis, with pyrite formation being inhibited by low permeability and consumption of available H_2S [6]. However, Roberts and Turner [6] reported that chlorite was a common constituent, in addition to greigite, in their magnetic extracts. It is therefore possible that this greigite formed during later diagenesis along with neoformed Fe-rich clays, as we have suggested for the Gutingkeng greigite studied here.

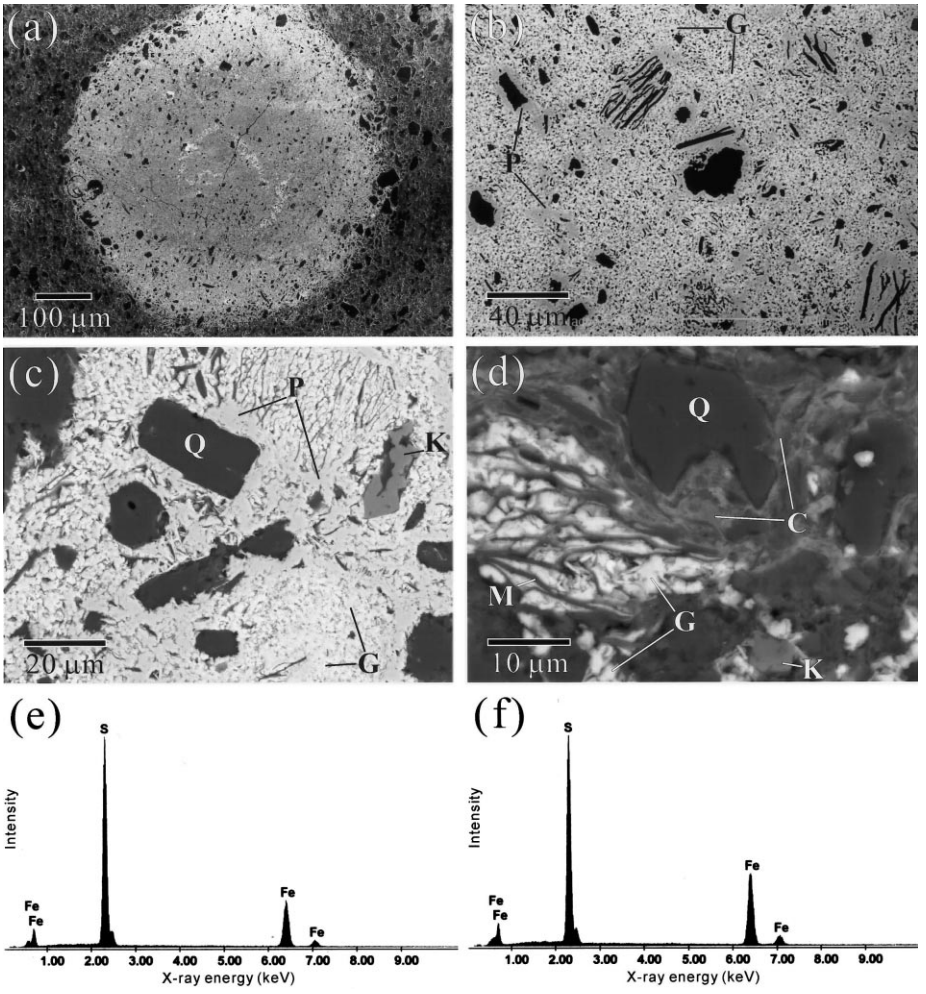

Fig. 7. Back scattered electron images of iron-sulfide nodules from the Gutingkeng mudstone. (a) A spherical iron-sulfide nodule in a silicate-dominated matrix (dark gray contrast) with the nodular core and rim dominated by pyrite (gray) and greigite (light gray), respectively. (b) Pyrite (gray; labeled P) and silicate (black) grains embayed by aggregates of small greigite crystals (light gray; G) within a nodule. (c) Pyrite grains (light gray; P) directly adjacent to partially dissolved silicate grains (gray and dark gray; Q = quartz; K = potassium feldspar), with dissolved edges in contact with greigite (bright; G) within a nodule. (d) Intergrowth of greigite (bright; G) and diagenetic clays (light gray; C) which partially replace a detrital muscovite grain (gray; M) in the vicinity of an iron-sulfide nodule. (e, f) X-ray energy-dispersive spectra of pyrite and greigite, respectively, obtained from an iron-sulfide nodule.

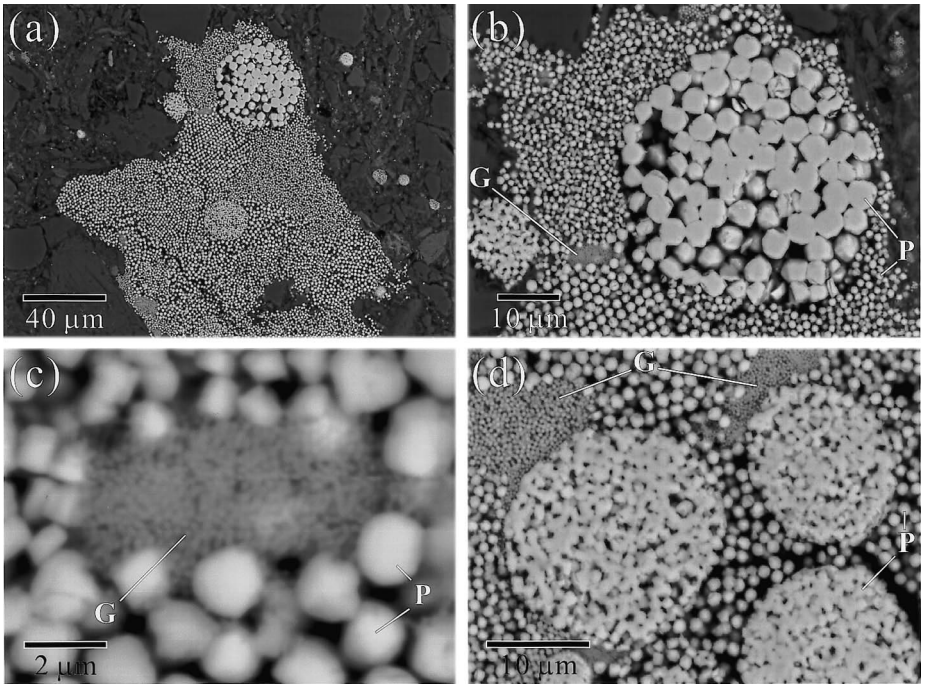

Fig. 8. BSE images of iron-sulfide aggregates and framboids from the Gutingkeng mudstone. (a) Irregular aggregates of iron sulfides (bright contrast) surrounding pyrite framboids (brightest). The surrounding dark areas are mostly silicates. (b) Intergrowth of aggregates of pyrite crystals of variable sizes (bright; labeled P) with coarser-grained framboidal pyrite (brightest; P). G = greigite. (c) Ultra-fine-grained greigite (gray; G) within the pyrite aggregate (bright; P) shown in (b). (d) Irregular patches of fine-grained greigite (gray; G) display irregular boundaries within pyrite aggregates (bright; P) and occur around the peripheral regions of pyrite framboids.

In the Simpson Oil field, Alaska, epigenetic greigite formation was related to sulfate supplied by hydrocarbon seepage [3–5]. Observations of greigite that formed substantially later than early burial (i.e. after establishment of a detrital magnetization) will have significant implications for the timing of remanence acquisition in greigite-bearing sediments.

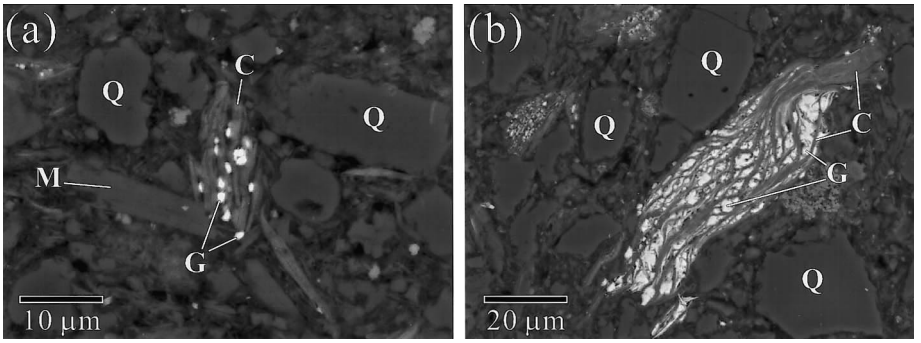

Fig. 9. BSE photomicrographs of the Gutingkeng mudstone. (a) Arrays of greigite grains (bright contrast; labeled G) occur along chlorite {001} cleavages (labeled C) and are surrounded by other silicate minerals (dark gray; M = muscovite; Q = quartz) in the matrix. (b) A chlorite grain (C) with spaces between distorted {001} cleavages filled by greigite aggregates (bright; G). Small bright spots in the matrix are also greigite. Q = quartz.

4.4. Paleomagnetic implications of greigite formation

A widely recognized formation sequence for sedimentary iron-sulfide minerals is as follows: cubic/noncrystalline monosulfides → mackinawite → greigite → pyrite/marcasite [2,30]. A high level of supersaturation with respect to iron sulfides favors formation of monosulfides and greigite, which subsequently transform into pyrite. The reaction sequence is not only suggested by geological evidence but is also directly supported by low-temperature laboratory synthesis [31,32]. These processes occur during early diagenesis at shallow burial depths. The greigite formed in this manner should therefore record a near-depositional polarity.

The NRMs carried by greigite in some of the Gutingkeng samples reported here exhibit paleomagnetic polarities that are sometimes opposite to those recorded by sister samples at the same stratigraphic level (Fig. 6), as was also shown for the Tsailiao-chi section where detrital magnetite exhibits dissolution pits and invariably shows normal polarity consistent with depositional age [9]. The contradictory magnetic polarity signals imply that the Gutingkeng greigite could have formed during diagenesis at depth after syngenetic or early diagenetic formation of pyrite. The microtextural evidence shown in this study strongly supports this interpretation. The contradictory polarities recorded either by different greigite components or by greigite and detrital components, respectively, are apparently dependent on the time lag between greigite formation and depositional age. The studied sediments have an early Pliocene depositional age that corresponds to the Gilbert Chron. Geomagnetic polarity reversals were relatively frequent in the Gilbert Chron. In sediment samples such as the Gutingkeng mudstone, where parts of the NRM were acquired at different times, frequent polarity reversals could produce composite NRMs that are occasionally consistent (i.e. all components have the same polarity) or occasionally inconsistent. That is, a later diagenetic magnetization carried by greigite could have either a normal or reversed polarity, as could the depositional magnetization (carried by detrital minerals or by early diagenetic greigite). Thus, documentation of consistent polarities at stratigraphic horizons containing neoformed greigite does not guarantee that a near-depositional early diagenetic polarity has been recorded.

4.5. Iron sources for diagenetic greigite

The neoformation of greigite after pyrite formation is apparently related to a change in physicochemical conditions. Formation of pyrite, especially framboidal pyrite, is favored by high concentrations of dissolved sulfide species with Fe available from reactive iron oxyhydroxides or oxides [2,23,24,30]. The Fe source for pyrite formation is most likely provided primarily by dissolution of detrital magnetite in the Gutingkeng mudstone. The concentration of magnetite must have therefore decreased with time and the concentration of sulfidic sulfur must have lowered as it was taken up by crystallization of pyrite. The pyrite subsequently experienced partial dissolution and greigite formed concurrently or later when the diagenetic processes involving P, T and redox changes and reactions between Fe- and S-bearing species reached a physicochemical state that was suitable for greigite formation. The fact that only little or no magnetite was detected in greigite-rich mudstones, and that magnetite is relatively abundant in greigite-poor or -barren samples of the Lower Gutingkeng formation supports this interpretation [9,11,12]. Although there are no published results on hydrocarbon migration in the region, the common occurrence of mud volcanoes associated with hydrocarbon-bearing fluids and gas suggests the possible existence of hydrocarbon activity, which may have caused changes in redox and chemical conditions that resulted in greigite formation within the Gutingkeng mudstone, as was the case in the Simpson Oil field, Alaska [3–5]. Detrital chlorite apparently provided sites for nucleation of matrix greigite and part of the available iron was derived from chlorite, as implied by common intergrowths of greigite with detrital chlorite.

Local overgrowth of pyrite by greigite is implied because the concretionary pyrite has partially dissolved edges and is embayed by greigite

aggregates. Also, the iron-sulfide nodules invariably have pyrite-dominated cores and greigite-enriched rims, implying replacement from rim toward core by interaction with pore fluids. Pyrite is generally a relatively stable phase in marine sediments, but it can be oxidized to form magnetite during oxic diagenesis [33,34]. It has been suggested that pyrite could react with oxidizing acids and other oxidants such as Fe^{3+} and molecular halogens [26]. The nodular greigite could have formed as a result of partial oxidation and dissolution of pyrite. The occurrence of neoformed iron-rich clays only in the vicinity of iron-sulfide nodules is consistent with the release of iron and sulfur from such a process. The released sulfur and iron may have provided material for the formation of other textural types of greigite elsewhere in the sediment. The general absence of sharp crystal edges in the framboidal pyrite also implies some degree of pyrite dissolution. These data collectively suggest that the neoformation of greigite was associated with diagenetic oxidation and dissolution of pyrite.

5. Conclusions

In this study, we have shown that greigite occurs in nodular, framboidal and matrix forms in mudstones from the Lower Gutingkeng Formation, southwestern Taiwan. The nodular greigite is intergrown with partially dissolved pyrite grains within iron-sulfide nodules that have greigite-dominated rims. The framboidal greigite fills intergranular space within pyrite aggregates, whereas the matrix greigite occurs between phyllosilicate layers or is dispersed in the sediment matrix. We infer that these three types of greigite formed during late diagenesis after syngenetic or early diagenetic formation of pyrite. Framboidal and matrix greigite probably formed via dissolution and neoformation processes, but nodular greigite was a replacement product of early-formed nodular pyrite involving oxidation/dissolution and neocrystallization. These different modes of diagenetic greigite formation give rise to NRMs that are often anti-parallel to the NRMs carried by detrital magnetic minerals or even by greigite within the same stratigraphic horizon. It is likely that similar mechanisms are responsible for other contradictory polarity records given by greigite and magnetic detrital minerals, as reported in the literature from several other locations. Direct petrographic observation of authigenic magnetic iron sulfides, as performed in this study, provides important constraints on the timing of magnetizations carried by such minerals. These results suggest that care should be taken to constrain the formation mechanisms of greigite in a given situation before attempting to interpret the paleomagnetic direction in terms of a near-depositional early diagenetic signal.

Acknowledgements

We thank Dr. Masayuki Torii for making the low-temperature IRM measurements at the Okayama University of Science, Japan, and for his comments on the manuscript. We are grateful to Leonardo Sagnotti and Martin Schoonen for their constructive reviews of the manuscript. This study was supported by the National Science Council of the Republic of China under Grants NSC89-2116-M-006-019 to W.T.J., NSC89-2911-I-001-082-2 and NSC91-2911-I-001-001 to C.S.H., by a grant from the Royal Society of London to A.P.R., and by National Science Foundation Grant EAR 9814391 to D.R.P. *[RV]*

References

[1] R.A. Berner, Sedimentary pyrite formation, Am. J. Sci. 268 (1970) 1–23.
[2] R.A. Berner, Sedimentary pyrite formation: an update, Geochim. Cosmochim. Acta 48 (1984) 605–615.
[3] R.L. Reynolds, N.S. Fishman, M.R. Hudson, Sources of aeromagnetic anomalies over Cement oil field (Oklahoma), Simpson oil field (Alaska), and the Wyoming–Idaho–Utah thrust belt, Geophys. 56 (1991) 606–617.
[4] R.L. Reynolds, M.B. Goldhaber, M.L. Tuttle, Sulfidization and magnetization above hydrocarbon reservoirs, Applications of Paleomagnetism to Sedimentary Geology, SEPM Spec. Publ. 49, 1993, pp. 167–179.
[5] R.L. Reynolds, N.L. Tuttle, C.A. Rice, N.S. Fishman, J.A. Karachewski, D.M. Sherman, Magnetization and geochemistry of greigite-bearing Cretaceous strata, North Slope Basin, Alaska, Am. J. Sci. 294 (1994) 485–528.

[6] A.P. Roberts, G.M. Turner, Diagenetic formation of ferrimagnetic iron sulphide minerals in rapidly deposited marine sediments, South Island, New Zealand, Earth Planet. Sci. Lett. 115 (1993) 257–273.
[7] D.F. Hallam, B.A. Maher, A record of reversed polarity carried by the iron sulphide greigite in British early Pleistocene sediments, Earth Planet. Sci. Lett. 121 (1994) 71–80.
[8] F. Florindo, L. Sagnotti, Palaeomagnetism and rock magnetism in the upper Pliocene Valle Ricca (Rome, Italy) section, Geophys. J. Int. 123 (1995) 340–354.
[9] C.-S. Horng, M. Torii, K.-S. Shea, S.-J. Kao, Inconsistent magnetic polarities between greigite- and pyrrhotite/magnetite-bearing marine sediments from the Tsailiao-chi section, southwestern Taiwan, Earth Planet. Sci. Lett. 164 (1998) 467–481.
[10] C.-S. Horng, K.-S. Shea, Study of nannofossil biostratigraphy in the eastern part of the Erhjen-chi section, southwestern Taiwan, Spec. Publ. Cent. Geol. Surv. 8 (1994) 181–204.
[11] C.-S. Horng, J.C. Chen, T.Q. Lee, Variation in magnetic minerals from two Plio–Pleistocene marine-deposited sections, southwestern Taiwan, J. Geol. Soc. China 35 (1992) 323–335.
[12] C.-S. Horng, C. Laj, T.Q. Lee, J.C. Chen, Magnetic characteristics of sedimentary rocks from the Tsengwen-chi and Erhjen-chi sections in southwestern Taiwan, Terrestrial Atmospheric and Oceanic Sciences 3 (1992) 519–532.
[13] M.J. Dekkers, J.-L. Mattéi, G. Fillion, P. Rochette, Grain-size dependence of the magnetic behavior of pyrrhotite during its low-temperature transition at 34 K, Geophys. Res. Lett. 16 (1989) 855–858.
[14] P. Rochette, G. Fillion, J.-L. Mattéi, M.J. Dekkers, Magnetic transition at 30–34 Kelvin in pyrrhotite: insight into a widespread occurrence of this mineral in rocks, Earth Planet. Sci. Lett. 98 (1990) 319–328.
[15] Ö. Özdemir, D.J. Dunlop, B.M. Moskowitz, The effect of oxidation on the Verwey transition in magnetite, Geophys. Res. Lett. 20 (1993) 1671–1674.
[16] M. Torii, K. Fukuma, C.-S. Horng, T.Q. Lee, Magnetic discrimination of pyrrhotite- and greigite-bearing sediment samples, Geophys. Res. Lett. 23 (1996) 1813–1816.
[17] M. Krs, F. Novák, M. Krsová, P. Pruner, L. Koukílková, J. Jansa, Magnetic properties and metastability of greigite-smythite mineralization in brown-coal basins of the Krusne Hory Piedmont, Bohemia, Phys. Earth Planet. Inter. 70 (1992) 273–287.
[18] A.P. Roberts, Magnetic properties of sedimentary greigite (Fe_3S_4), Earth Planet. Sci. Lett. 134 (1995) 227–236.
[19] L. Sagnotti, A. Winkler, Rock magnetism and palaeomagnetism of greigite-bearing mudstones in the Italian peninsula, Earth Planet. Sci. Lett. 165 (1999) 67–80.
[20] R.T. Wilkin, H.L. Barnes, Formation processes of framboidal pyrite, Geochim. Cosmochim. Acta 61 (1997) 323–339.
[21] J. Sellés-Martínez, Concretion morphology, classification and genesis, Earth Sci. Rev. 41 (1996) 177–210.
[22] R. Raiswell, Pyrite texture, isotopic composition and the availability of iron, Am. J. Sci. 282 (1982) 1244–1263.
[23] R. Raiswell, R.A. Berner, Pyrite formation in euxinic and semi-euxinic sediments, Am. J. Sci. 285 (1985) 710–724.
[24] D.E. Canfield, R.A. Berner, Dissolution and pyritization of magnetite in anoxic marine sediments, Geochim. Cosmochim. Acta 51 (1987) 645–659.
[25] D.E. Canfield, R. Raiswell, S.H. Bottrell, The reactivity of sedimentary iron minerals toward sulfide, Am. J. Sci. 292 (1992) 659–683.
[26] D. Rickard, M.A.A. Schoonen, G.W. Luther, III, The chemistry of iron sulfides in sedimentary environments, in: V. Vairavamurthy, M.A.A. Schoonen (Eds.), Geochemical Transformations of Sedimentary Sulfur, American Chemical Society Symposium Series 612, 1995, pp. 168–193.
[27] R.T. Wilkin, H.L. Barnes, Pyrite formation in an anoxic estuarine basin, Am. J. Sci. 297 (1997) 620–650.
[28] K.G. Taylor, J.H.S. Macquaker, Early diagenetic pyrite morphology in a mudstone-dominated succession: the Lower Jurassic Cleveland Ironstone Formation, eastern England, Sediment. Geol. 131 (2000) 77–86.
[29] E. Tric, C. Laj, C. Jéhanno, J.-P. Valet, C. Kissel, A. Mazaud, S. Iaccarino, High-resolution record of the upper Olduvai transition from Po Valley (Italy) sediments: support for dipolar transition geometry?, Phys. Earth Planet. Inter. 65 (1991) 319–336.
[30] R.A. Berner, Thermodynamic stability of sedimentary iron sulfides, Am. J. Sci. 265 (1967) 773–785.
[31] M.A.A. Schoonen, H.L. Barnes, Reactions forming pyrite and marcasite from solution: I. Nucleation of FeS_2 below 100°C, Geochim. Cosmochim. Acta 55 (1991) 1495–1504.
[32] M.A.A. Schoonen, H.L. Barnes, Reactions forming pyrite and marcasite from solution: II. Via FeS precursors below 100°C, Geochim. Cosmochim. Acta 55 (1991) 1505–1514.
[33] L.A. Brothers, M.H. Engel, R.D. Elmore, The late diagenetic conversion of pyrite to magnetite by organically complexed ferric iron, Chem. Geol. 130 (1996) 1–14.
[34] S. Banerjee, R.D. Elmore, M.H. Engel, Chemical remagnetization and burial diagenesis: testing the hypothesis in the Pennsylvanian Belden Formation, Colorado, J. Geophys. Res. 102 (1997) 24825–24842.